HHS Public Access

Author manuscript

Int J Min Sci Technol. Author manuscript; available in PMC 2019 November 01.

Published in final edited form as:

Int J Min Sci Technol. 2018 November ; 28(6): 969–974. doi:10.1016/j.ijmst.2018.05.010.

Evaluation of fiber optic methane sensor using a smoke chamber

Mingming Li*, **Thomas Dubaniewicz**, **Heather Dougherty**, and **Jim Addis**

National Institute for Occupational Safety and Health, Pittsburgh Mining Research Division, Pittsburgh 15236, USA

Abstract

This report presents the results of experiments to evaluate a prototype fiber optic methane monitor exposed to smoke using a smoke chamber to simulate atmospheric conditions in an underground coal mine after a fire or explosion. The experiments were conducted using test fires of different combustible sources commonly found in mines —douglas-fir wood, SBR belt, and Pittsburgh seam coal. The experiments were designed to assess the response of the fiber optic methane sensor to different contaminants, different contaminant levels and different contaminant durations produced from the test fires. Since the prototype methane monitor detects methane by measuring absorption at a specific wavelength, optical power at the absorption wavelength (1650 nm) was measured as a function of smoke concentration and duration. The other sensor response parameter-methane response times-were measured between smoke tests to assess the impact of soot accumulation on the sensor. Results indicate that the sensor screen effectively prevented smoke from obscuring the optical beam within the sensor head, with minimal impact on the system optical power budget. Methane response times increased with smoke exposure duration, attributed to soot loading on the protective screen.

Keywords

Fiber optic; Methane sensor; Fires; Optical power; Response time

1. Introduction

Underground mining has historically been recognized as one of the most hazardous occupations in the United States. Because many coal mines liberate great quantities of methane, potential explosion hazards can develop due to accumulation of high methane levels. Although less frequent in modern times, methane-related mining accidents are often disastrous. This is most recently evidenced by the Upper Big Branch Mine explosion in 2010, which originated from a longwall face methane ignition, then transitioned into a small methane explosion that propagated into a massive coal dust explosion, resulting in the deaths

*Corresponding author. limingming.lmm@gmail.com (M. Li).

Disclaimer

The findings and conclusions in this paper are those of the authors and do not necessarily represent the views of the National Institute for Occupational Safety and Health (NIOSH). Mention of any company or product does not constitute endorsement by NIOSH.

of twenty-nine miners. A ventilation system is one of the essential components to ensure a safe and healthy environment in underground coal mines, providing oxygen for humans and diluting hazardous gases and dust. In order for the ventilation system to accomplish these important tasks, it should be managed, maintained, and monitored effectively. In addition to the regular examinations and maintenance of the ventilation system, the continuous atmospheric monitoring of the key parameters can be helpful for early detection of potential hazards. Methane has always been one of the critical parameters.

Historically, the methane sensor primarily used in coal mines is the catalytic bead sensor. This sensor contains a coil of wire embedded in a glass or ceramic material that is coated with a catalyst [1]. When monitoring a hydrocarbon combustible gas, the coil is electrically heated, causing the gas to burn at a certain temperature and producing heat that is proportional to the gas concentration, resulting in a temperature rise that increases the resistance of the coil. A catalytic bead sensor is electrically powered and has to comply with MSHA intrinsic safety requirements to avoid spark ignition of explosive gases in a mining environment. Catalytic sensors are limited to the measurement of methane concentrations that fall in the range from 0 to 5% [2]. Catalytic sensors also rely on catalytic combustion to detect a combustible gas and require a minimum of 12% atmospheric oxygen for proper operation, which may not be present during mine emergency atmospheric conditions [2]. Moreover, another consideration for a catalytic sensor is the sensitivity to higher hydrocarbons such as ethane and propane, and other flammable gases such as hydrogen [3].

As an alternative to the catalytic bead sensor, fiber optic sensors are electrically passive and may be ideally suited for deployment in isolated and remote areas in mines, such as sealed areas, belt entries, and pillar recovery sections. The use of such technology could enable quicker detection and response to avoid potentially hazardous conditions. Because of recent advances in research and development of fiber optic technology, fiber optic sensing has been introduced in the mining industry for various applications, such as strain sensing, distributed temperature sensing, and gas detection [4,5]. A number of studies investigated the use of fiber optic sensors to monitor methane [6–9].

Recently, a fiber optic-based methane monitor was developed under a Pittsburgh Mining Research Division (PMRD) extramural contract with RSL Fiber Systems LLC [10]. The system utilizes a 10 milliwatt (mW) diode laser at a wavelength around 1650 nm in conjunction with a distributed fiber network and a series of ruggedized sensor modules. The optical absorption sensing technique does not rely on oxygen being present in the atmosphere as is the case with catalytic bead sensors. Thus, high levels of methane (above the upper explosive limit in air), or lower levels of methane in oxygen deficient atmospheres, may be monitored with the fiber optic system. These features would be particularly useful during emergencies initially caused by fires or explosions. The RSL system is specified to measure methane levels from 0.5% to 100%. The three main components of the RSL system —a central control unit, optical fiber, and fiber optic sensor head—are shown in Fig. 1. Fiber optic connectors are used to attach the fiber optic cable to the remote sensor and central control unit. Fig. 2 shows the inside components of the optic sensor head (bottom) and the dust screen (top). The optical methane sensor head detects methane in the air cavity between the lenses via the absorption of one of the diode laser-generated wavelengths. The dust

screen is a cylindrical shape metal tube that covers the fiber optic sensor to protect the sensing components from being damaged. The main part of the dust screen is made of fine metal mesh. Gases can flow through the dust screen and enter into the air cavity, allowing the fiber optic sensor to detect methane.

RSL conducted a series of laboratory and in-mine tests to examine the sensor's reliability and durability [10]. The laboratory controlled tests conditions included high humidity, high rock dust concentrations, and vibration. RSL also performed in-mine tests subjecting the methane sensors to the conditions of a working underground coal mine [10]. However, the in-mine test conditions reflected normal gas concentrations expected under normal mine operation. The suitability of the system for underground application during emergency atmospheric conditions caused by fire or explosion has not been investigated. Post-event situations may present atmospheres contaminated with combustion products such as smoke, carbon monoxide, and carbon dioxide. In the current work, researchers with the National Institute for Occupational Safety and Health (NIOSH), Pittsburgh Mining Research Division (PMRD) assessed the performance of the RSL fiber optic monitor exposed to smoke from combustion of three common materials found in coal mines: douglas-fir wood, SBR belt, and Pittsburgh seam coal.

2. Experimental details

Combustion experiments were conducted using an Underwriters Laboratories, Inc. (UL 268) smoke chamber. Connected to the smoke chamber is a combustion chamber which contains a circular disk heater used to heat the solid combustibles (Fig. 3). This system was developed and validated previously by Perera and Litton [11]. Three combustible materials were used in the experiments to generate smoldering fires: wood chips from dried douglas-fir, Pittsburgh seam coal (−20 to +30 mesh), and styrene butadiene rubber (SBR) from a non-fire-resistant conveyor belt.

A TSI DustTrak 8520 was used for continuous measurement of the aerosol mass concentrations. Inside the smoke chamber, the optical density of the aerosol was measured over a 1.48 m optical path length using an incandescent lamp and a standard photocell with spectral response matching the spectral response of the human eyes [11]. In addition, a small laser and silicon photodiode was used to measure the light extinction over a 0.65 m path at a wavelength of 532 nm. Metal tubes were placed at the top of the smoke box to extract aerosols from the smoke chamber that flowed to various measuring devices. The temperature inside the smoke chamber was measured using a thermocouple, and the humidity inside the chamber was obtained using a Lascar EL-USB-2-LCD temperature and humidity data logger.

The combustible materials were heated until they burned on a hot plate. The smoke was mixed uniformly using two small circulating fans in the smoke chamber. A vane anemometer was installed inside a metal tube connected to the combustion chamber to measure the air velocity flowing into the chamber (shown in Fig. 3). For all of the experiments, the combustion materials were heated for 20–25 min to produce continuous smoke. Smoke generation started 3–5 min after starting the hot plate. Smoke concentration,

directly measured by the TSI DustTrak, increased dramatically for approximately 4–6 min and then dropped after reaching peak values. After smoke generation returned to a low concentration (less than 10 mg/m^3), the fires were allowed to burn for another 5 min before being extinguished. The circulating fans were then used to clear the smoke from the smoke chamber before another experiment was initiated. Fig. 4 shows a diagram of the smoke exposure experiment setup.

During the experiments, the RSL fiber optic methane sensor was placed perpendicular to the front face of the smoke chamber through a hole located in the upper center of the front face (Figs. 3 and 4). Three RSL fiber optic methane sensor heads were used in the experiments—one per combustible material.

A Keysight Technologies Inc. model 8163 B dual channel Multimeter with two Keysight 81623B optical heads was used to monitor 1650 nm light split off from the RSL fiber optic methane sensor while it was exposed to smoke (Fig. 5). One channel monitored the light transmitting through the smoke-exposed sensor, and the other channel monitored a portion of the light transmitting through a fiber optic splitter not exposed to smoke. The dual channel power meter measurements monitored optical power fluctuations due to the smoke exposure while accounting for potential light source power fluctuations. Any measured optical power fluctuations due to smoke exposure would impact the optical power budget of the total fiber optic loop.

Researchers used an RSL supplied gas calibration tube to measure the methane response before and after each FO methane sensor was exposed to smoke (Fig. 6). The FO methane sensor (with the dust screen) was placed inside the cylindrical tube with calibration gas flow into the tube. The gas flow rate was adjusted to produce an initial response time of approximately 60 s for a clean sensor. The sensor response time will be different for different gas flow rates and different test procedures; thus the response times reported here for clean sensors are different than those specified by the manufacturer. T90 response times (sensor reading reaching 90% of full gas scale) for a 2.97% CH_4-air calibration gas source, i.e., 2.67% CH_4-air, were recorded. In order to measure the impact of smoke exposure over time, the sensor was exposed to smoke during four subsequent smoke exposure tests with the same combustible material for approximately 20–25 min. The response time was measured immediately after each smoke exposure. The monitor reading reached 2.67% CH_4-air for all tests.

3. Results and discussion

3.1. Combustion tests

For each combustible source—douglas-fir wood, SBR belt, and Pittsburgh seam coal—four tests were performed in the smoke chamber, resulting in twelve combustion tests in total. Table 1 summarizes each combustion test including mass of the combustible material, temperature and humidity in the smoke chamber, and air velocity flowing into the combustion chamber. The combustible materials were carefully weighed before and after each test. The douglas-fir wood burned completely with little ash while the SBR belt and Pittsburgh seam coal were burnt incompletely with a certain amount of remains. The mass of

wood burned in each test was approximately 5 g for all four combustion tests. For the SBR rubber, the mass differences before and after combustion ranged from 1.92 to 4.16 g, and the mass for Pittsburgh seam coal burnt in each test was between 1.13 and 1.65 g. Temperature in the smoke chamber was found to increase with smoke duration. The smoke usually resulted in several degrees of temperature rise except for the first test of SBR belt. The humidity inside the smoke chamber ranged from 23% to 49%. The air velocity was maintained around 0.91 m/s for each test except for douglas-fir-2 test, which was 1.10 m/s.

3.2. Aerosol mass concentrations

The Dusttrak is a convenient way to measure aerosol mass concentration continuously. However, application of dusttrak is limited when the aerosol mass concentration exceeds the maximum measurement range of the dusttrak (150 mg/m^3). Thus the optical density, a function of mass concentration, is to be used to compute the mass concentrations in this study. As mentioned previously, both the broadband visible light and monochromatic electromagnetic radiation at wavelength 532 nm were used to measure the light extinction data. The light transmission through a homogeneously dispersed cloud of uniform dust particles can be expressed as Eq. (1) [12]. The mass concentration of smoke aerosols can be then computed using Eq. (2).

$$\frac{I}{I_0} = e^{-\sigma_{ext} \cdot m \cdot l} \quad (1)$$

where I is the transmitted irradiance; I_0 the incident irradiance; σ_{ext} the extinction coefficient; m the mass concentration, g/m^3; and l the path length, m.

$$m = -\frac{1}{\sigma_{ext} \cdot l}\left(\ln \frac{I}{I_0}\right) \quad (2)$$

While there is always some interference in the visible obscuration data from forward scattering (not purely extinction) for the obscuration meter, light extinction measured at the 532 nm wavelength is not affected similarly, and the smoke mass concentrations can be calculated reliably from 532 nm extinction data. The light extinction varies depending on the type of combustion or the mode of combustion due to differences in particle size, morphology, and chemistry [11]. Thus, the extinction coefficient is a critical parameter to determine the aerosol mass concentration produced from different combustible materials. Perera and Litton conducted research to calculate the mass absorption, mass extinction, and mass scattering coefficients for aerosols from both flaming and non-flaming combustion [11]. The mass extinction coefficients measured at 532 nm for non-flaming combustion for douglas-fir, SBR belt, and Pittsburgh coal are 7.594, 8.272, and 7.036, respectively.

Fig. 7 indicates the changes of mass concentration vs time from the 532 nm extinction data for the SBR belt. The sensor exposure to smoke of the particular combustible source could

be varied by both the time duration and smoke mass concentration. These two parameters may affect the sensor performance in optical power and/or the sensor response time. In order to calculate the cumulative smoke mass, M_{CUM}, that the sensor is exposed to, the following equation was used.

$$M_{CUM} = \sum_{t=0}^{t=t(\max)} (m \times \Delta t) \quad (3)$$

where M_{CUM} is the cumulative smoke exposure, mg-s/m^3; m the mass concentration, mg/m^3; and t the time sensor exposed to smoke, s. All the calculations in the study were acquired in a similar manner.

The smoke concentrations for experiments from different combustible sources are summarized in Table 2. Smoke concentration varies depending on type and weight of combustible sources. Compared to the other two combustible sources, the SBR belt produced higher values of maximum smoke concentration and cumulative smoke exposure, which was also evidenced by the heavier smoke observed in the experiments. The cumulative smoke exposure for SBR belt was 2.84×10^5 mg-s/m^3, nearly double of the cumulative smoke exposure for douglas wood and Pittsburgh seam coal, which were 1.39×10^5 and 1.57×10^5 mg-s/m^3, respectively.

3.3. Optical power loss

3.3.1. Optical power loss vs time—The optical power loss is one of the critical measurements in characterizing the impact of smoke exposure to the optical power budget of the total fiber optic loop. As shown in Fig. 5, one channel of the power meter monitored light transmitting through the smoke-exposed sensor (P_2), and another channel monitored light transmitting through a fiber optic splitter not exposed to smoke (P_1). As mentioned previously, both channels monitored the light at 1650 nm. Since the splitter divided nearly equal optical power into the connected two optical fibers, the power transmitting before the smoke-exposed sensor (input optical power, P_{in}) is equal to the power measured by channel 1, and the power transmitting after the sensor (output optical power, P_{out}) is double the optical power measured by channel 2. Using the relationship $P_{in} = P_1$ and $P_{out} = 2P_2$, the input and output optical power of the sensor can be obtained. Optical power loss can be calculated using Eq. (4) [13].

$$dB = 10 \log (P_{mea}/P_{ref}) \quad (4)$$

where P_{mea} is the measured power level, mW; and P_{ref} the reference power level, usually 1 mW for an optical system.

$$\Delta dB = dB(in) - dB(out) \quad (5)$$

where ΔdB is the optical power loss budget, dB; $dB(in)$ the input optical power in decibel, dB; and dB(out) the output optical power in decibel, dB.

Fig. 8 shows the variation of optical power loss vs time for the douglas-fir-2 test. The initial optical power loss was about 6.67 dB. Since the fiber optic methane sensor was not exposed to smoke for the first 180 s, the initial optical power loss only refers to transmission path losses through the test setup (Fig. 5). After putting the sensor into the smoke box, the optical power loss jumped to about 6.72 dB—a 0.05 dB increase. This small step increase in loss may be due to slight beam alignment changes as the sensor and fiber optic connections were manipulated into place within the smoke chamber. The total optical power loss gradually increased to about 6.74 dB after 20 min of smoke exposure. In Fig. 8, an upper bound for the optical power loss due to smoke attenuation is approximately 0.08 dB. This result indicates that, for the douglas-fir-2 test, the optical power loss caused by smoke attenuation was very small. Similar trends of optical power loss were found for most of the 12 tests using the three different combustible sources—a jump of 0.04–0.05 dB after putting the sensor into the smoke box, then a small power loss changes during smoke exposure.

Table 3 summarizes the transmission path loss, total power loss, and maximum power loss due to smoke exposure. The transmission path loss was different for different sensors, which was around 7 dB for sensors used in the wood and belt combustion tests, and around 12 dB for the sensor used in the coal combustion tests. The maximum power loss due to smoke attenuation was between 0.02 and 0.08 dB for the wood tests and between 0.01 and 0.07 dB for the belt tests. The maximum power loss due to smoke attenuation for the coal tests ranged from 0.03 to 0.07 dB. The RSL system is specified to tolerate signal losses of up to 90% [10]. The optical power loss due to smoke attenuation was minimal compared to the system loss tolerance.

3.3.2. Optical power loss vs smoke concentration—The variation of optical power loss vs smoke concentration for the douglas-fir-2 test is shown in Fig. 9. The highest smoke concentration was 122 mg/m^3 during this test. The total power loss values were scattered from 6.71 to 6.76 dB. The upper limit of the optical power loss remained around 6.76 dB, while the lower limit increased from 6.71 to 6.72 dB as the smoke concentration increased. The data scatters of the optical power loss vs smoke concentration were observed for other smoke tests with different combustible sources as well. However, similar increases of the lower limit of optical power loss were not found in all the tests, only in the douglas-fir-2 and Pittsburgh seam coal tests. Furthermore, since the increase of the lower limit of optical power loss was only 0.01 dB, it was unclear whether there was any obvious correlation between the smoke concentration and optical power loss. The lack of obvious correlation between smoke concentration and optical power loss suggests that a majority of the loss was due to other factors. Slight beam alignment changes as the sensor and fiber optic connections were manipulated into place within the smoke chamber are a likely explanation.

3.4. Methane response

In order to evaluate the impact of soot accumulation on the protective screen, the T90 response time to a 2.97% CH_4-air calibration gas source was measured after each smoke exposure test. Fig. 10 shows T90 response times vs the duration of smoke exposure for the douglas-fir wood, Pittsburgh seam coal, and SBR rubber. As mentioned previously, the calibration gas flow was adjusted to produce a T90 response time of approximately 60 s for a clean sensor. Fig. 10 shows that sensor response time correlates with smoke duration very well, with linear regressions for all three sensors exposed to different combustible sources. In the wood smoke tests, sensor response time increased to 67.5 s after 70 min of smoke exposure. In the belt smoke and coal smoke tests, sensor response time increased to 70.5 s and 68.1 s after 100 min of smoke exposure, respectively. The increases in sensor response time are probably because exposure to smoke coats the sensor screen with particulate matter.

The response time of the fiber optic methane sensor is also presented as a function of the cumulative smoke exposure, which refers to both smoke duration and smoke concentration. Fig. 11 shows that, for all three sensors, sensor response time increased linearly with the sensor's cumulative smoke exposure. For sensors exposed to smoke from douglas-fir wood and Pittsburgh coal, the sensor response time vs cumulative smoke exposure were very close to each other. But for the sensor exposed to smoke from the SBR belt, the response time increased more slowly with smoke exposure than that of the sensors exposed to smoke from wood and coal. The reason could be that the SBR belt generated a higher smoke concentration over a shorter time period. Fig. 11 also suggests that the SBR belt smoke blocked the screen to a lesser extent than the coal or wood smoke for a given exposure. As mentioned previously, the SBR belt generated a smoke amount nearly double of that from the other two combustible sources (Table 2). However, there was no significant differences between the response time for sensor exposed to belt smoke and that exposed to wood or coal smoke when the sensors were exposed to smoke for a given time. Even though the SBR belt generated a much larger amount of smoke, apparently the SBR smoke did not adhere as well to the sensor screen.

3.5. Discussion

Comparing the optical loss and methane response time results suggest that soot accumulation on the screen may have a greater impact than smoke occluding the optics under longer-duration exposure conditions. The SBR belt material did not appear to adhere to the screen as well as the other materials. Results suggest that one potential area for further research is an assessment of smoke adhering properties of candidate screening materials. It should be noted that the fires were relatively small in these smoke chamber tests. Less than 5 g of combustion material was burned in each test, and the highest temperature in the smoke chamber was 95 °F. An actual mine fire would generate much greater smoke amounts and higher temperatures than studied here. The results of this study are encouraging and warrant further research to assess the performance of the fiber optic methane sensor under more severe smoke and temperature conditions representative of a larger scale fire or explosion.

4. Conclusions

The ability to monitor methane remotely within oxygen deficient, contaminated atmospheres may be extremely beneficial during mine emergencies involving initial fires or explosions. A prototype remote fiber optic methane monitor was challenged with combustion smoke from three representative coal mine materials—namely douglas-fir wood, SBR belt, and Pittsburgh seam coal. A protective screen covering the fiber optic sensor effectively prevented smoke from obscuring the optical beam under specified test conditions. The sensor response time increased linearly with smoke duration for the three combustible materials, attributed to loading of soot on the protective screen. Comparing the optical loss and methane response time results suggest that soot accumulation on the screen may have a greater impact than smoke occluding the optics under longer-duration exposure conditions. Further research is warranted to assess the performance of the fiber optic methane sensor under more severe smoke and temperature conditions representative of a larger scale fire or explosion. The performance assessment of the fiber optic methane sensor during smoke exposure in this study can be used toward the modification and application of fiber optic sensing technologies that will be beneficial for mine safety, particularly for post-disaster situations.

Acknowledgments

The authors would like to acknowledge John Soles and Richard Thomas at the National Institute for Occupational Safety and Health (NIOSH), Pittsburgh, PA, for their help with the smoke chamber tests.

References

1. Chaulya SK, Prasad GM. Sensing and monitoring technologies for mines and hazardous areas. 1. UK: Elsevier; 2016.
2. Valoski MP. Instruments for gas analysis at mine fires/explosions. SME Preprint. 2010:10–039.
3. Hartman HL, Mutmansky JM, Ramani RV, Wang YJ. Mine ventilation and air conditioning. 3. New York: John Wiley & Sons; 1997.
4. Xu S, Zhang P, Zhang D, Wu R, Guo L. Simulation study of fiber optic monitoring technology of surrounding rock deformation under deep mining conditions. J Civ Struct Health Monitor. 2015; 5(5):563–71.
5. Dubaniewicz T, Kovalchik P, Scott L, Fuller M. Distributed measurement of conductor temperatures in mine trailing cables using fiber-optic technology. IEEE Trans Ind Appl. 1998; 34(2):395–8.
6. Dubaniewicz TH, Chilton JE. Report of Investigations 9407. United States Bureau of Mines; 1992. Remote fiber-optic mine methane monitor.
7. Tong M, Niu J, Hao J, Jia C. Study on a fiber optic sensor for CH4 in mine. Proceedings 2010 symposium on photonics and optoelectronic; 2010;
8. Shemshad J, Aminossadati SM, Kizil MS. A review of developments in near infrared methane detection based on tunable diode laser. Sens Actuators, B. 2012; 171–172:77–92.
9. Shemshad J, Aminossadati SM, Kizil M, Bowen W, Kizil M. Effects of pressure and temperature fluctuations on near-infrared measurements of methane in underground coal mines. Appl Phys B: Laser Opt. 2012; 106(4):979–86.
10. RSL Fiber System LLC. RSL Final Technical Report. 2012. Method for improving ventilation and gas and temperature monitoring with an advanced fiber optic-based mine wide monitoring system.
11. Perera IE, Litton CD. Quantification of optical and physical properties of combustion-generated carbonaceous aerosols (< $PM_{2.5}$) using analytical and microscopic techniques. Fire Technol. 2015; 51(2):247–69. [PubMed: 27546898]

12. Perera IE, Litton CD. A detailed study of the properties of smoke particles produced from both flaming and non-flaming combustion of common mine combustibles. Fire safety science-proceedings of the tenth international symposium; 2011;

13. Krohn DA, MacDougall T, Mendez A. Fiber optic sensors: fundamentals and applications. 4. Bellingham: Spie Press; 2014.

Fig. 1.
RSL fiber optic methane detection system.

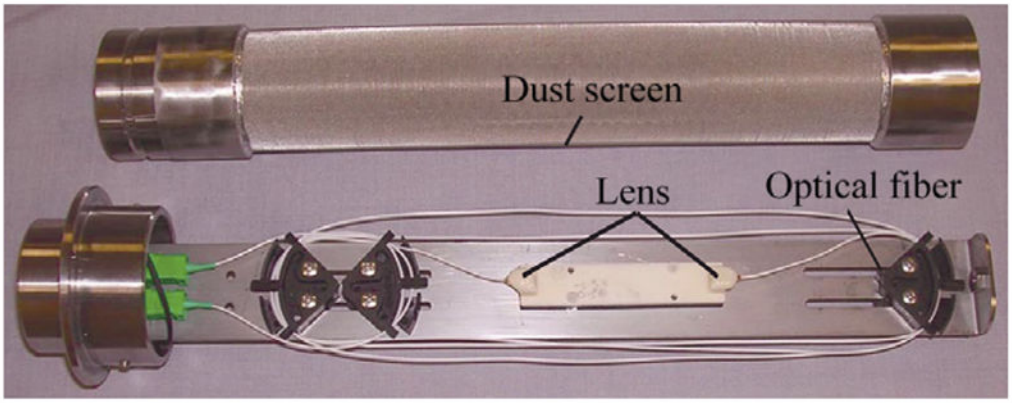

Fig. 2.
Remote optical methane detector shown with and without dust screen [10].

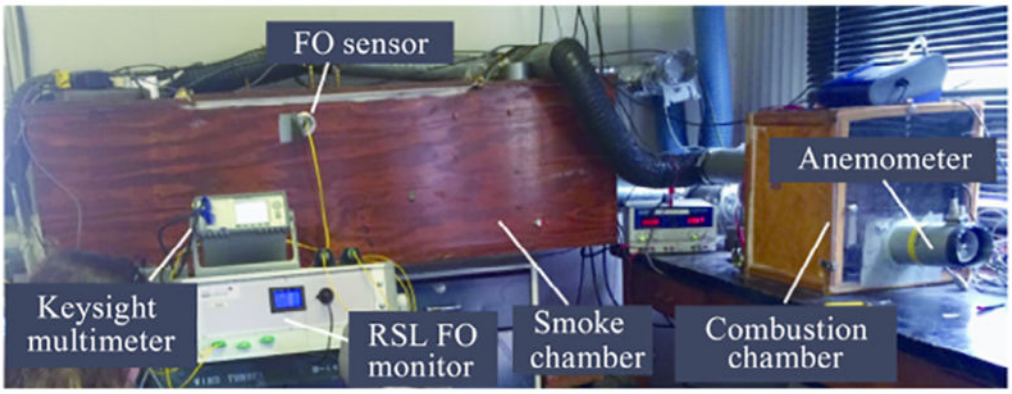

Fig. 3.
Smoke exposure experiment in smoke chamber.

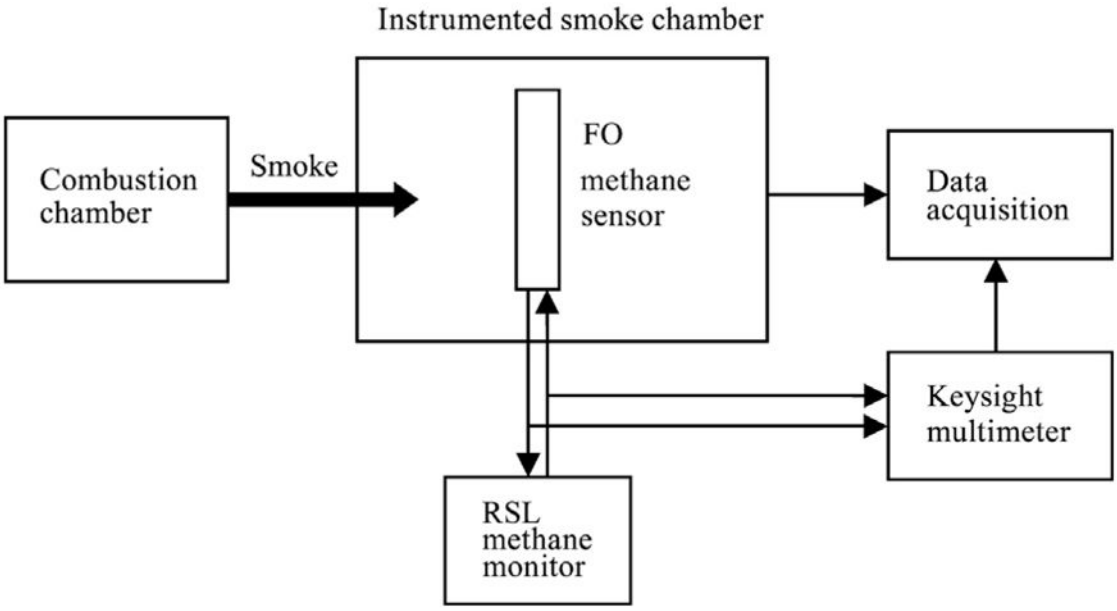

Fig. 4.
Diagram of the smoke exposure experiment setup.

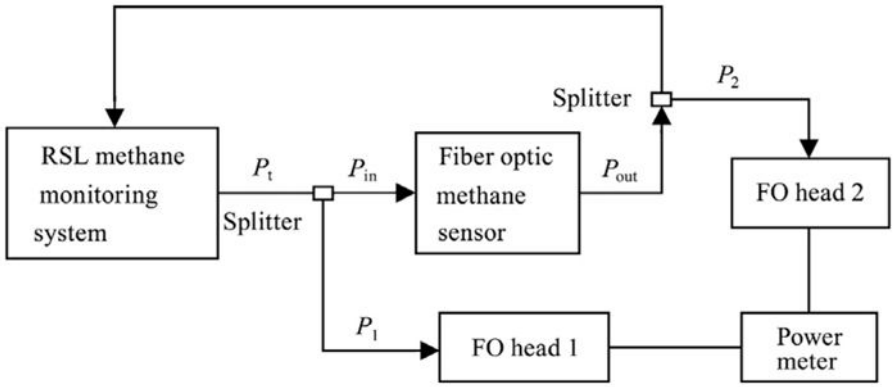

Fig. 5.
Equipment configuration for optical power measurement.

Fig. 6.
Cylindrical tube and fiber optic sensor.

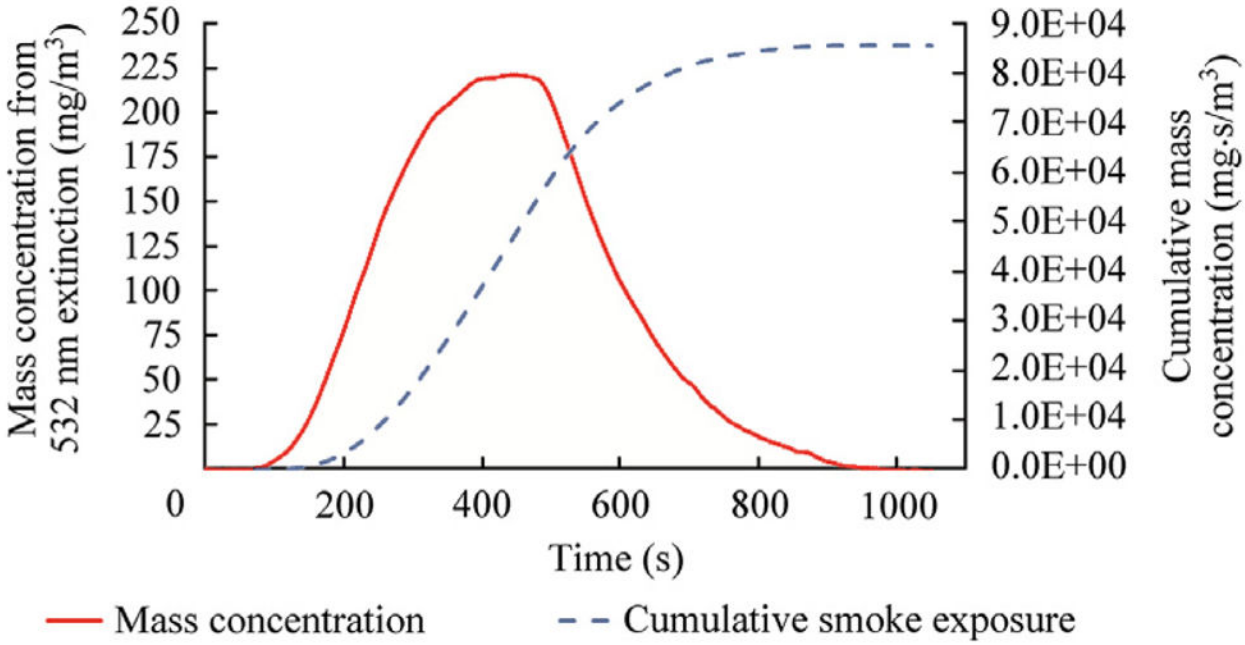

Fig. 7.

Variation of mass concentration vs time and cumulative mass concentration for SBR belt-1.

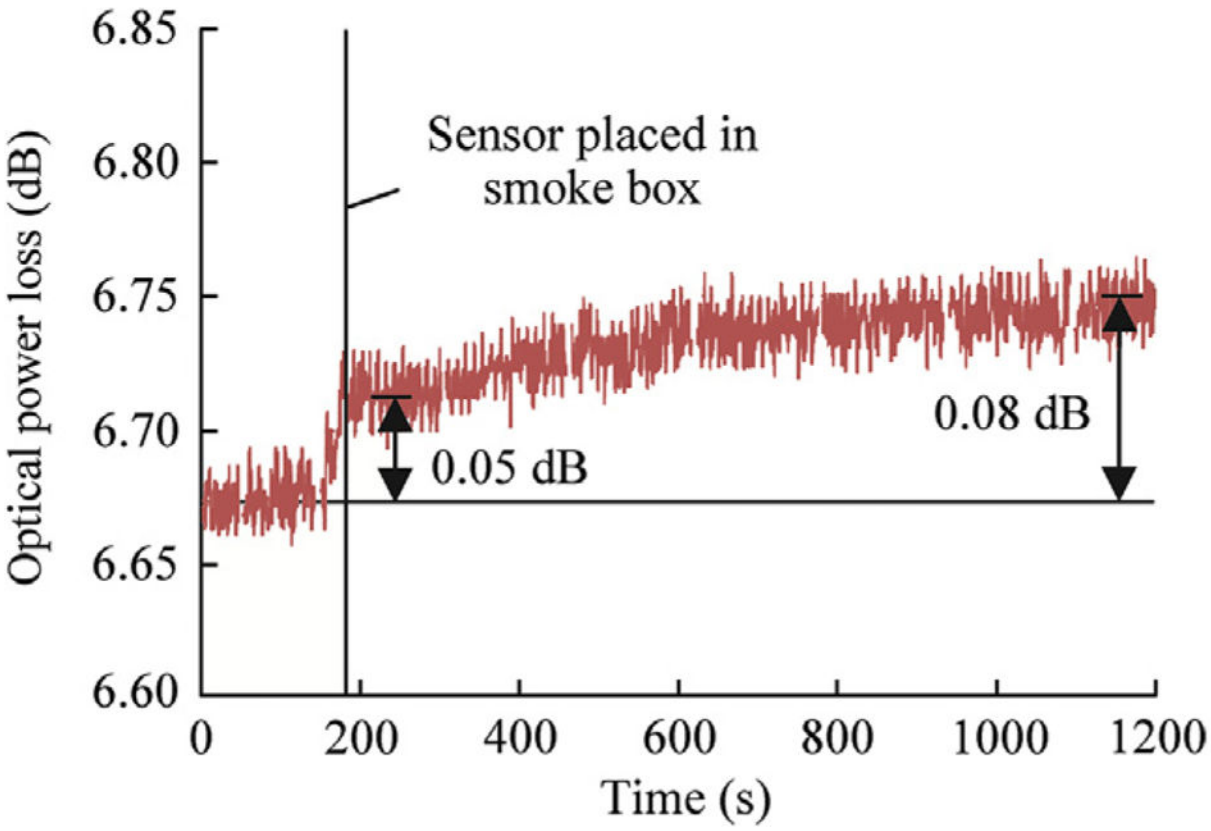

Fig. 8.
Variation of optical power loss vs time for Douglas-fir-2 test.

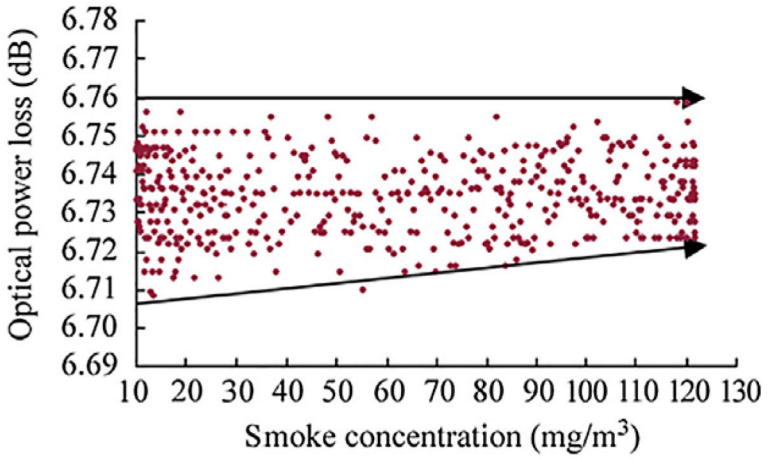

Fig. 9.
Variation of optical power loss vs smoke concentration for douglas-fir-2 test.

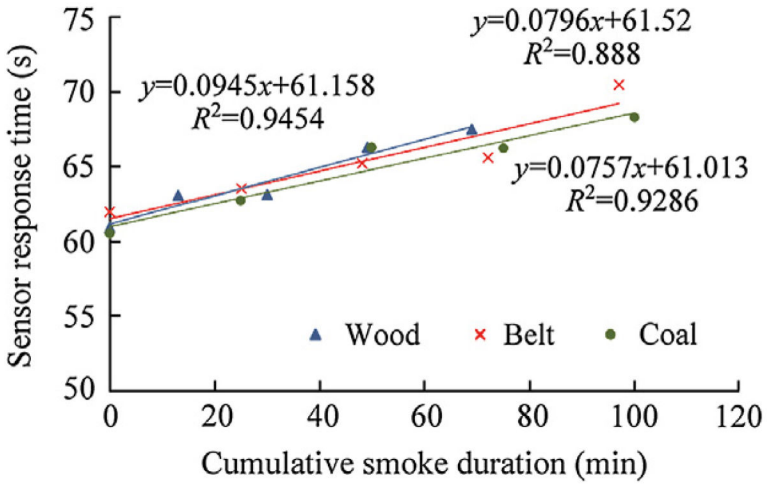

Fig. 10.
Sensor response time vs cumulative smoke duration for different combustion sources.

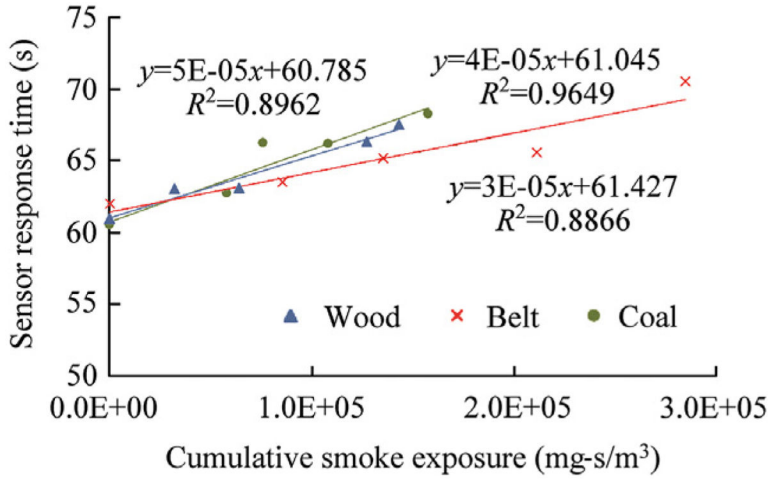

Fig. 11.
Sensor response time vs cumulative smoke exposure for different combustion sources.

Table 1

Mass of combustion materials and test conditions for different combustion tests.

Item	Weight before burning (g)	Weight after burning (g)	Δ weight (g)	Lowest temperature (°F)	Highest temperature (°F)	Temperature rise (°F)	Average humidity (%)	Air velocity (m/s)
glas-fir-1	4.95	0.00	4.95	82.4	88.9	6.50	49.3	0.96
Douglas-fir-2	4.90	0.00	4.90	83.8	93.6	9.80	39.9	1.10
Douglas-fir-3	5.15	0.00	5.15	84.3	93.2	8.90	35.4	0.92
Douglas-fir-4	4.95	0.00	4.95	87.2	92.8	5.60	32.7	0.98
SBR belt-1	14.4	10.2	4.16	82.8	83.6	0.80	30.9	0.92
SBR belt-2	4.98	3.06	1.92	83.2	90.9	7.70	30.9	0.96
SBR belt-3	6.44	3.35	3.09	80.8	93.5	12.7	30.5	0.93
SBR belt-4	7.75	4.58	3.17	84.5	94.9	10.4	28.0	0.93
Pgh seam coal-1	9.40	7.75	1.65	78.6	83.2	4.60	28.9	0.89
Pgh seam coal-2	4.99	3.86	1.13	81.4	85.3	3.90	25.3	0.90
Pgh seam coal-3	7.27	6.07	1.20	80.3	84.0	3.70	25.1	0.92
Pgh seam coal-4	8.04	6.86	1.18	83.1	88.0	4.90	23.1	0.92

Table 2

Smoke concentration and cumulative smoke exposure for different combustion tests.

Item	Average smoke concentration (mg/m^3)	Maximum smoke concentration (mg/m^3)	Duration of smoke exposure (min)	Cumulative smoke exposure (mg-s/m^3)
Douglas-fir-1	57	164	13	3.19E+04
Douglas-fir-2	37	122	17	3.19E+04
Douglas-fir-3	56	124	19	5.97E+04
Douglas-fir-4	16	62	20	1.60E+04
Douglas-fir total				1.39E+05
SBR belt-1	75	221	25	8.56E+04
SBR belt-2	43	136	23	4.95E+04
SBR belt-3	55	167	24	7.59E+04
SBR belt-4	50	174	25	7.34E+04
SBR belt total				2.84E+05
Pgh seam coal-1	42	114	25	5.81E+04
Pgh seam coal-2	12	35	25	1.76E+04
Pgh seam coal-3	22	68	25	3.22E+04
Pgh seam coal-4	39	96	25	4.95E+04
Pgh seam coal total				1.57E+05

Table 3

Optical power loss when sensor was exposed to smoke of different combustible sources.

Item	Average transmission path loss (dB)	Maximum loss (dB)	Maximum loss due to smoke attenuation (dB)
Douglas-fir-1	7.07	7.09	0.02
Douglas-fir-2	6.67	6.75	0.08
Douglas-fir-3	7.10	7.12	0.02
Douglas-fir-4	7.02	7.05	0.03
SBR belt-1	7.18	7.21	0.03
SBR belt-2	6.83	6.90	0.07
SBR belt-3	6.87	6.84	0.03
SBR belt-4	7.14	7.15	0.01
Pgh coal-1	11.9	11.8	0.07
Pgh coal-2	12.1	12.1	0.03
Pgh coal-3	11.9	11.8	0.06
Pgh coal-4	11.7	11.6	0.05